11-25-2014

Mesoscale Convective System Surface Pressure Anomalies Responsible for Meteotsunamis Along the U.S. East Coast on June 13th, 2013

Christina A. Wertman

Richard M. Yablonsky

Yang Shen
University of Rhode Island, y.shen@icloud.com

John Merrill
University of Rhode Island, jmerrill@uri.edu

Christopher R. Kincaid
University of Rhode Island, kincaid@uri.edu

See next page for additional authors

Citation/Publisher Attribution

Wertman CA, Yablonsky RM, Shen Y, Merrill J, Kincaid CR, Pockalny RA. (2014). "Mesoscale convective system surface pressure anomalies responsible for meteotsunamis along the U.S. East Coast on June 13th, 2013." Scientific Reports. 4: 7143.
Available at: http://dx.doi.org/10.1038/srep07143

Mesoscale Convective System Surface Pressure Anomalies Responsible for Meteotsunamis Along the U.S. East Coast on June 13th, 2013

Authors

Christina A. Wertman, Richard M. Yablonsky, Yang Shen, John Merrill, Christopher R. Kincaid, and Robert A. Pockalny

SCIENTIFIC REPORTS

OPEN

SUBJECT AREAS:
PHYSICAL OCEANOGRAPHY
ATMOSPHERIC DYNAMICS

Received
24 February 2014

Accepted
21 October 2014

Published
25 November 2014

Correspondence and requests for materials should be addressed to Y.S. (yshen@gso.uri.edu)

Mesoscale convective system surface pressure anomalies responsible for meteotsunamis along the U.S. East Coast on June 13th, 2013

Christina A. Wertman, Richard M. Yablonsky, Yang Shen, John Merrill, Christopher R. Kincaid & Robert A. Pockalny

Graduate School of oceanography, University of Rhode Island, Narragansett, RI 02882, USA.

Two destructive high-frequency sea level oscillation events occurred on June 13th, 2013 along the U.S. East Coast. Seafloor processes can be dismissed as the sources, as no concurrent offshore earthquakes or landslides were detected. Here, we present evidence that these tsunami-like events were generated by atmospheric mesoscale convective systems (MCSs) propagating from inland to offshore. The USArray Transportable Array inland and NOAA tide gauges along the coast recorded the pressure anomalies associated with the MCSs. Once offshore, the pressure anomalies generated shallow water waves, which were amplified by the resonance between the water column and atmospheric forcing. Analysis of the tidal data reveals that these waves reflected off the continental shelf break and reached the coast, where bathymetry and coastal geometry contributed to their hazard potential. This study demonstrates that monitoring MCS pressure anomalies in the interior of the U.S. provides important observations for early warnings of MCS-generated tsunamis.

Tsunamis are most often caused by sudden movement of the seafloor due to submarine earthquakes, landslides, or volcanic activities. Tsunami-like events created by disturbances on the ocean surface are less well known, but their existence is well-documented in areas such as the Balearic Islands, the Adriatic Sea, South Japan, New Zealand, northeastern North America, the United Kingdom, and northwestern North America[1–5]. Common to all of these ocean surface-generated tsunami-like events is forcing by an atmospheric surface pressure anomaly moving over a relatively shallow body of water[3]. Hence, this type of tsunami-like event is typically classified as a "meteotsunami".

A large sea level anomaly associated with a meteotsunami can occur through a variety of atmosphere-ocean resonance mechanisms, including Greenspan, Shelf, and/or Proudman resonance[3]; for the meteotsunamis examined in the current study, Proudman resonance has the largest influence on the sea level anomaly. Proudman resonance exists when the ground speed of the atmospheric pressure anomaly (U) matches the phase speed of meteotsunami waves (C), which travel as shallow water waves so that $C = (gh)^{1/2}$, where g is the gravitational acceleration (9.8 m s^{-2}) and h is the water depth[6]. For an atmospheric pressure anomaly propagating at a common ground speed of 20–40 m s^{-1}, the corresponding resonant water depth is 40–160 m, within the depth range of most continental shelves.

Although not widely known, meteotsunamis along the east coast of North America are not rare events. There have been at least two documented meteotsunami events each year with sea level oscillations of 0.1–1 m along the U.S. East Coast from 2006 to early 2012, although the atmospheric forcing for these meteotsunamis has not been investigated in detail[7,8]. Mercer et al.[2] describes two tropical cyclones, Helene (2000) and Jose (1999), which generated meteotsunamis (with wave heights up to 3m) as the low-pressure anomalies at the center of the tropical cyclones rapidly propagated across the Grand Banks. These meteotsunamis then reflected back toward the coast once the storms crossed the shelf break into deeper water. Since limited observations of the pressure distributions in the tropical cyclones were available, Mercer et al.[2] estimated the pressure distribution using a simple analytical model.

Tropical cyclones do not appear to be the most common cause of meteotsunamis along the U.S. East Coast. Churchill et al.[9] describes a mesoscale convective system (MCS), which propagated southward along the east coast

of Florida, generating a 3-m meteotsunami (recorded at Daytona Beach) that was forced by a high surface pressure anomaly under the squall line portion of the MCS. They used hourly radar reflectivity and barometric pressure readings from sparse stations to illustrate the relationship between radar reflectivity and the high atmospheric pressure anomaly. Churchill et al.[9] recorded a positive pressure anomaly of ~2 hPa, and through their estimations of atmospheric forcing, they concluded that, in addition to Proudman resonance, bathymetric effects (including wave refraction off an underwater ridge) may have played a large role in generating such a high amplitude meteotsunami.

Some MCSs include a fast-moving, long-lived, quasi-linear squall line (i.e., derecho), which produces strong winds and has a well-defined surface pressure anomaly signature (Fig. 1a). Derecho-producing MCSs are not uncommon in the interior of the U.S., numbering on average ~20 per year with a possible upward trend in frequency[10]. Most common in the months of May, June, and July, derechos frequently occur in groups along the eastern half of the U.S.[10,11]. On land, the most destructive impact of a derecho-producing MCS is typically straight-line wind damage, but as the MCS passes over the ocean, the potential initiation of a meteotsunami creates a different hazard.

On June 13, 2013, two high-frequency sea level oscillation (i.e., meteotsunami) events hit the U.S. East Coast. The maximum sea level oscillations recorded at National Oceanic and Atmospheric Administration (NOAA) tide gauges for the first and second meteotsunamis were 0.59 m at Providence, RI and 0.44 m at Atlantic City, NJ, respectively (i.e., stations 27 and 19, respectively, in Table 1 and Supplementary Fig. 1). Earthquakes and landslides can be dismissed as the likely causes of these events because no earthquake was detected near the coast around the times of the events, and a subsequent offshore survey near Hudson Canyon by NOAA found no evidence of a significant submarine landslide (Jason Chaytor, personal communication). However, two derecho-producing MCSs propagated eastward off the U.S. East Coast that same day[12] (Fig. 2). Using recently available barometric pressure measurements from the USArray Transportable Array (TA) and radar reflectivity with high temporal sampling, this study builds upon previous studies (such as Churchill et al.[9]) by quantitatively documenting and analyzing the atmospheric surface pressure anomalies associated with MCSs that generate meteotsunamis along the U.S. East Coast. Similar concurrent MCS-meteotsunami pairs occurred along the U.S. East Coast on June 29–30, 2012 and April 10–11, 2013 (see Supplementary Figs. 2 and 3), but for brevity, the focus here is on the June 13, 2013 event.

Results

MCS atmospheric pressure anomalies. Two sets of instruments are used to measure the atmospheric pressure on the Earth's surface during the two eastward-propagating MCSs on June 13, 2013. Unlike previously documented U.S. East Coast meteotsunami events, barometers on the recently installed TA stations in the eastern U.S. were available to record atmospheric surface pressure anomalies over land at a sample rate of once per second[13]. These measurements provided the first detailed account of the magnitude, dimension, and duration of the atmospheric pressure anomalies that were ultimately responsible for the meteotsunamis along the U.S. eastern seaboard, once the pressure anomalies moved offshore. Along the coast, NOAA tide gauges are used to monitor sea level, but many also measure coincident atmospheric sea level pressure, with 0.1 hPa precision and a six-minute sampling frequency[14] (Table 1 and Supplementary Fig. 1). All barometric pressure anomalies are calculated by demeaning the recorded pressure values and then high-pass filtering above five hours to highlight the high-frequency pressure anomalies (Fig. 1).

A derecho-producing MCS typically includes a quasi-linear group of thunderstorms, consisting of well-developed convective and stratiform cloud regions. Since radar measures reflectivity off water and ice particles, areas with the heaviest precipitation, such as beneath the convective towers (i.e., squall line) in a MCS, have the highest reflectivity, as shown in Fig. 1. In a well-developed MCS, the downdraft is often directly below this area of high reflectivity, creating a meso-high[15]. In addition to high pressure under the convective towers, warm air preceding the convective towers is forced upwards in the gust front, creating a precursory mesolow ahead of the mesohigh[15,16].

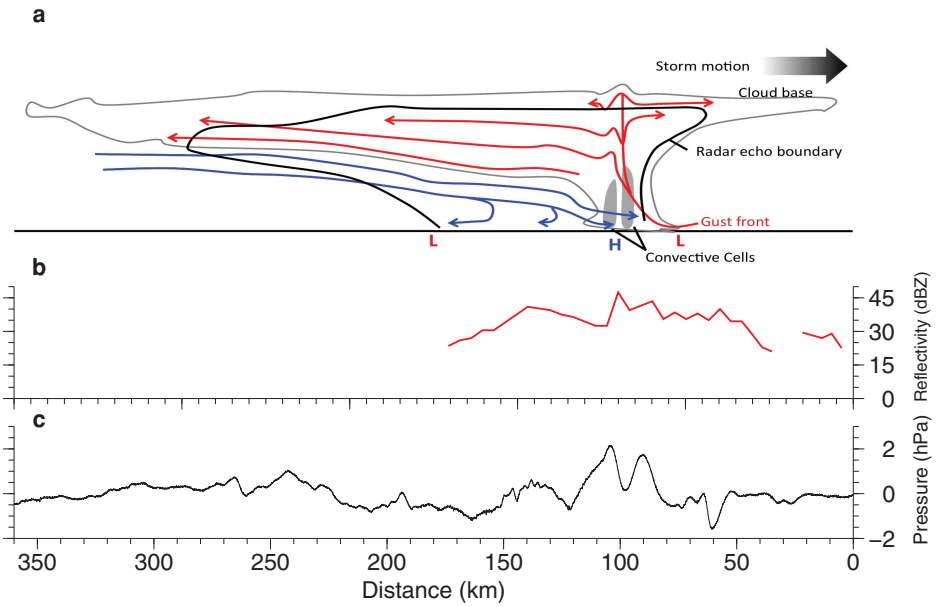

Figure 1 | Schematic, observed radar reflectivity, and observed surface pressure of the June 13, 2013 MCS at USArray station TA.P61A displayed in Figure 2 (Hammonton, NJ). (a) Vertical cross-section schematic of an MCS with a leading squall line and trailing stratiform region (adapted from Houze et al.[17]), where arrows indicate airflow, "L" markers indicate area of low surface pressure, and "H" marker indicates area of high surface pressure; (b) NOAA/WSR-88D radar station KDIX (Mt. Holly, NJ) base reflectivity (red) and (c) demeaned and five-hour high-pass filtered barometric pressure anomaly (black) from TA station P61A.

Table 1 | NOAA tide gauge and DART buoy locations and water depth. Gauge and buoy locations are mapped in Supplemental Figure 1

Station	Lat (N)	Long (W)	Mean Water Depth (m)	Station number	Location
8411060	44.66	−67.21	12.66	38	Cutler Farris Warf, ME
8413320	44.39	−68.21	9.14	37	Bar Harbor, ME
8418150	43.66	−70.25	13.49	36	Portland, ME
8419317	43.32	−70.56	19.53	35	Wells, ME
8423898	43.07	−70.71	7.41	34	Fort Point, NH
8443970	42.20	−71.05	8.73	33	Boston, MA
8447386	41.70	−71.16	23.06	32	Fall River, MA
8447435	41.69	−69.95	6.48	31	Chatham, MA
8449130	41.29	−70.10	3.6	30	Woods Hole, MA
8452660	41.51	−71.31	3.6	29	Newport, RI
8452944	41.72	−71.34	20.6	28	Conimicut Light, RI
8454000	41.81	−71.40	5.74	27	Providence, RI
8454049	41.86	−71.41	24.9	26	Quonset Point, RI
8461490	41.36	−72.09	5.06	25	New London, CT
8465705	41.28	−72.91	21.7	24	New Haven, CT
8467150	41.17	−73.18	5.6	23	Bridgeport, CT
8510560	41.05	−71.96	5.1	22	Montauk, NY
8518750	40.70	−74.01	5.86	21	The Battery, NY
8531680	40.47	−74.01	5.09	20	Sandy Hook, NJ
8534720	39.36	−74.42	7.17	19	Atlantic City, NJ
8536110	38.97	−74.96	4.99	18	Cape May, NJ
8537121	39.31	−75.38	21.42	17	Ship John Shoal, NJ
8557380	38.78	−75.12	5.01	16	Lewes, DE
8570283	38.33	−75.09	9.31	15	Ocean City Inlet, MD
8571421	38.22	−76.04	29.95	14	Bishops Head, MD
8571892	38.57	−76.07	3.48	13	Cambridge, MD
8575512	38.98	−76.48	5.24	12	Annapolis, MD
8577330	38.32	−76.45	4.48	11	Solomons Island, MD
8631044	37.61	−75.69	4.6	10	Wachapreague, VA
8635750	38.00	−76.46	5.53	9	Lewisetta, VA
8636580	37.62	−76.29	2.96	8	Windmill Point, VA
8637689	37.23	−76.48	6.44	7	Yorktown USCG Training Center, VA
8638863	36.97	−76.13	4.7	6	Chesapeake Bay Bridge Tunnel, VA
8639348	36.78	−76.30	23.18	5	Money Point, VA
8651370	36.18	−75.75	20.35	4	Duck, VA
8654467	35.21	−75.70	27.66	3	USCG Station Hatteras, NC
8656483	34.72	−76.67	3.55	2	Beaufort, NC
8662245	33.35	−79.19	6.66	1	Oyster Landing, SC
44402	39.40	−70.94	2443		DART 44402
41424	32.922	−72.466	5284		DART 41424

Also, another mesolow often follows the convective line in the stratiform region of the MCS (i.e., wake low), resulting from adiabatic warming of the descending air mass in the rear of the MCS[17]. This mesolow/mesohigh/mesolow pressure combination is well illustrated by TA station P61A as the first MCS passed over the coastline (Fig. 1). Here, the first mesolow pressure anomaly of −0.5 hPa corresponds to a narrow area of stratiform precipitation, indicated by moderate radar reflectivity. Immediately behind this first mesolow is an area of strong reflectivity, up to 45 dBZ, with a corresponding pressure anomaly of 2.8 hPa. Finally, as the reflectivity decreases to 20 dBZ, the pressure anomaly associated with the wake low reaches a minimum value of −1.8 hPa. The MCS creates a peak-to-trough anomaly of 4.6 hPa. Radar images from station KDOX show that the cross-sectional reflectivity of the first MCS extends about ~90 km front-to-back, roughly east-to-west, as the MCS passes over TA station P61A (Fig. 2e). While the highest reflectivity occurred concurrently with the highest positive pressure anomalies (Fig. 2a–d), the mesolow/high/low sequence may further enhance meteotsunami generation relative to a scenario whereby the precursor mesolow and wake low were not present. By examining many TA stations and NOAA tide gauges simultaneously, the highest pressure occurs beneath the MCS's convective squall line (Fig. 3), though interpolation of pressures at the stations broadens the apparent pressure anomaly along the convective line. The second MCS passed further south ~6 hours after the first MCS, arriving at Bishops Head, MD with an associated peak-to-trough pressure anomaly of ~5 hPa (Fig. 2d). The TA station O61A (Fig. 2a), which is located on the extreme northern fringe of the second MCS near the synoptic scale low pressure center, did not show significant atmospheric pressure anomalies and did not have reflectivity measurements above 40 dBZ.

The maximum peak-to-trough atmospheric pressure anomalies during the two MCSs at all of the TA stations and tide gauges are shown in Supplementary Fig. 4. The first MCS had a latitudinal footprint of 200 km. The maximum peak-to-trough pressure anomaly reached 6 hPa and remained stable at ~4 hPa as it passed over Delaware Bay. The second MCS had a larger latitudinal footprint of 500 km, and its largest maximum pressure anomaly recorded was far inland; as it traversed the Atlantic coast, the maximum pressure anomaly recorded by both TA stations and NOAA tide gauges was ~3 hPa. The magnitude of pressure anomalies across the interior of the U.S. illustrates the long duration and wide spatial coverage of these MCSs. It should also be noted that these surface pressure anomalies may be enhanced by atmospheric ducting[18], but the thermodynamic profiles in advance of the MCSs do not support ducting being a dominant mechanism for pressure anomaly generation in this case (Supplementary Figs. 5 and 6).

The maximum atmospheric pressure anomalies at the TA stations and tide gauges correlate with the peak radar reflectivity (Figs. 1–3). Three different methods are used to further confirm this observation. First, the collocation of the center of radar reflectivity and atmo-

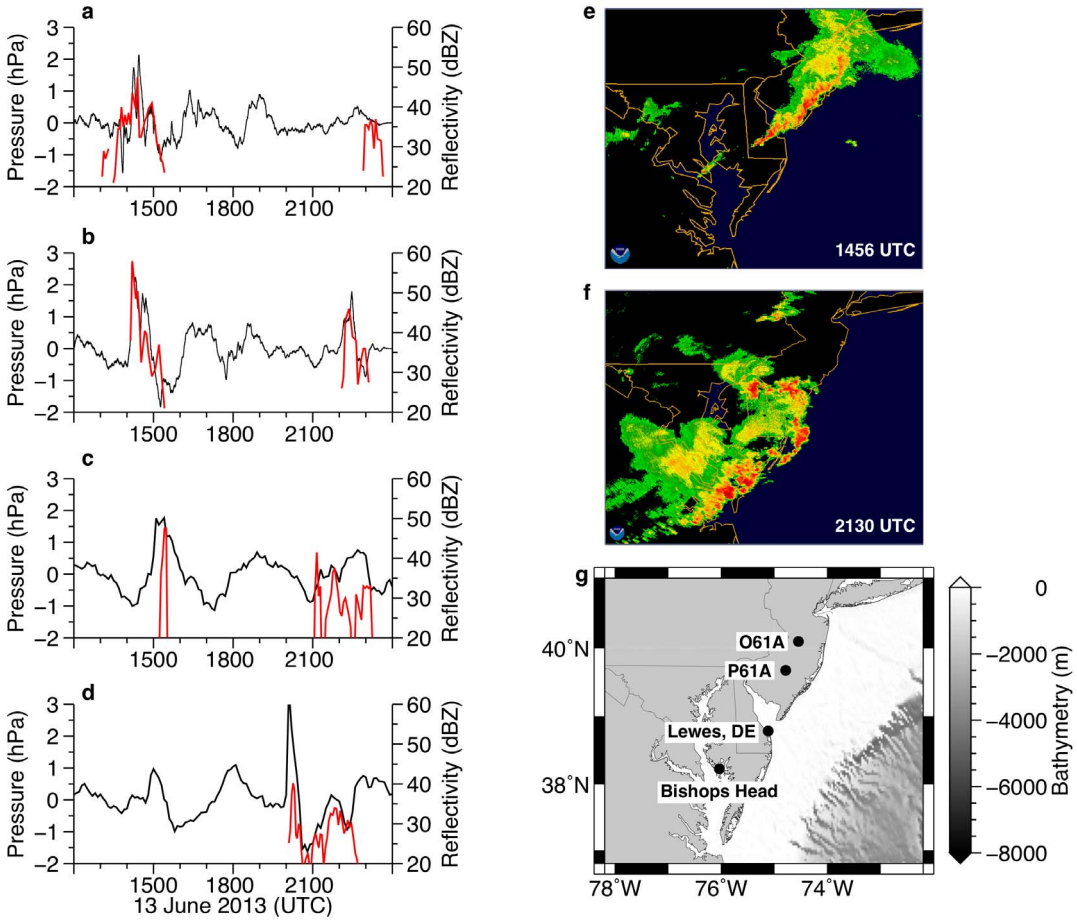

Figure 2 | Radar reflectivity and pressure comparison. Base radar reflectivity (red) and demeaned and five-hour high-pass filtered atmospheric pressure anomaly (black) for USArray stations (a) TA.O61A and (b) TA.P61A, as well as NOAA tide gauges in (c) Lewes, DE and (d) Bishops Head, MD, on June 13, 2013 (with time indicated in UTC); NOAA/WSR-88D NEXRAD radar station KDOX base reflectivity at (e) 1456 UTC (first MCS) and (f) 2130 UTC (second MCS), obtained using the NOAA Weather and Climate Toolkit; (g) map displaying locations of time series in (a) – (d). Maps (e) and (f) were created with software NOAA's Weather and Climate Toolkit (WCT v3.7.4; http://www.ncdc.noaa.gov/wct/). Map (g) was created with software Generic Mapping Tools (GMT v4.5.12; http://gmt.soest.hawaii.edu).

spheric pressure anomaly is verified, as shown in Supplementary Fig. 7 and described in the Method section. As the first MCS on June 13th,2013 moves across the interior of the United States, the position of the center of the atmospheric pressure anomaly is never more than 150 km away from the center of the radar reflectivity values. Second, to confirm that the storm moves at the same velocity as the atmospheric pressure anomaly, the propagation velocity derived from both radar reflectivity and atmospheric pressure anomalies is shown in Supplementary Fig. 8 and described in the Method section. While these propagation velocity estimations are within ~5 m/s of each other, closer agreement may be inhibited by the relatively coarse 70-km spacing of the TA stations, causing under sampling of the full field of the 150-km-wavelength atmospheric pressure anomaly. The estimation of the atmospheric pressure anomaly propagation velocity could be improved with decreased station spacing and/or modeling of the phenomenon. Finally, over a given continental location (in this case at TA stations), it is shown that the arrival of the maximum observed atmospheric pressure anomaly and the arrival of the maximum observed radar reflectivity occur at the same time (Supplementary Fig. 9), verifying that the average velocities of the MCS and pressure anomalies must be similar. These observations of location, speed, and timing provide the basis to infer MCS pressure anomalies offshore using radar reflectivity data, where direct atmospheric pressure measurements at sea level are currently lacking.

Once offshore, the propagation speeds and back-azimuths of the MCSs are estimated from radar reflectivity (Method). The first MCS maintained an average speed of 22 m/s as it propagated over the Atlantic Ocean at ~1500 UTC and dissipated by ~2000 UTC (Fig. 4). Conversely, the second MCS decelerated after ~0000 UTC on June 14 and was sustained for > 16 hours before the MCS propagated out of radar range.

Sea level response to atmospheric pressure anomalies. Spatial and temporal patterns in sea surface elevation from 38 NOAA tide gauge stations are analyzed to reveal meteotsunami generation and transport characteristics. Twenty-four hours of sea level records starting at 1200 UTC on June 13, 2013 are examined after the NOAA tide predictions have been removed[19] and the resulting demeaned data have been five-hour, high-pass filtered (Fig. 5a). The first tide gauge that recorded the first MCS was station 17 (Ship John Shoal, NJ; Table 1). Sea level oscillations at this station were small (< 0.2 m peak-to-trough). Larger sea level oscillations associated with the first MCS started at a tide gauge located in Lewes, DE (station 16; Table 1) at 1500 UTC, following within a few minutes of a ~3 hPa peak-to-trough pressure anomaly at the same location (Fig. 5; Supplementary Fig. 10). Stations to the south recorded more gradual pressure anomalies and undetectable sea level oscillations. To the north, station Cape May, NJ (station 18), also located in

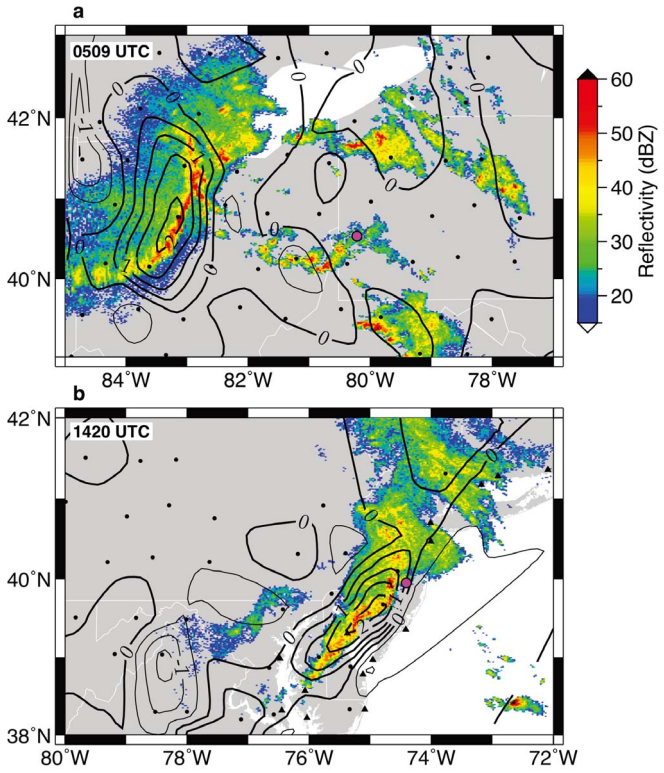

Figure 3 | Snapshots of atmospheric surface pressure anomaly and radar reflectivity during the first MCS. Contours of atmospheric surface pressure anomalies cubically interpolated from TA (circle) and tide gauge (triangle) stations at (a) 0509 UTC and (b) 1420 UTC, overlaid on base radar reflectivity images from NOAA/WSR-88D radar stations (a) KPBZ and (b) KDIX, with radar locations indicated by magenta circles. Positive (negative) pressure anomalies (in hPa) displayed by thick (thin) black lines. Maps were created with software Generic Mapping Tools (GMT v4.5.12; http://gmt.soest.hawaii.edu).

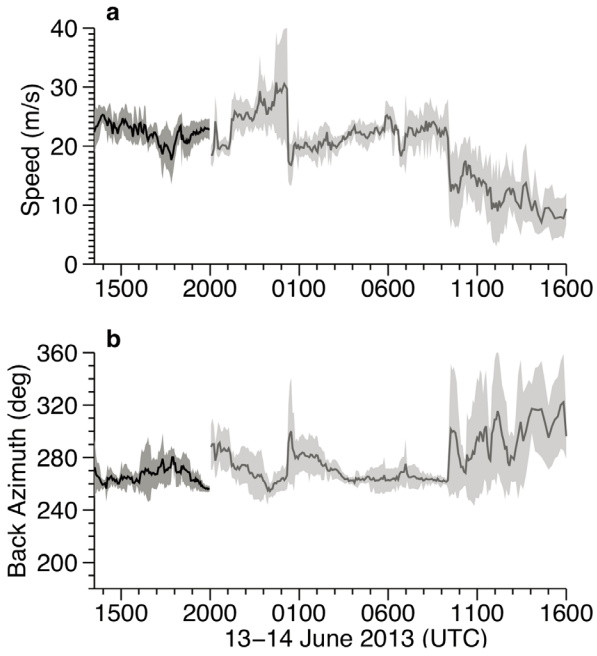

Figure 4 | Estimated (a) propagation speed and (b) back-azimuth for both MCSs. The speeds of the first MCS (black) and second MCS (gray) are calculated starting when the MCS moves over Chesapeake Bay and ending when the MCSs dissipate or are out of the range of land based radar. Time is in hours from 0000 UTC on June 13. The meteorological convention is used here, whereby the back-azimuth is the direction from which the disturbances originate.

Delaware Bay, detected a sea level oscillation beginning at ~1500 UTC but with a peak-to-trough pressure anomaly of ~4 hPa arriving ~20 minutes earlier at ~1440 UTC (Supplementary Fig. 10). Sea level oscillation arrivals north of Cape May display a lag time of up to 3 hours relative to pressure anomalies. Such is the case at Atlantic City, NJ (station 19), for which a pressure anomaly arrived at 1500 UTC but the first sea level oscillation did not arrive until 1806 UTC. Stations north of the Montauk, NY (station 22) tide gauge did not measure a significant atmospheric pressure anomaly but had significant sea level oscillations. Newport, RI (station 29), for example, had a maximum peak-to-trough sea level oscillation of ~0.5 m but no significant atmospheric pressure anomaly. Maximum sea level oscillations and atmospheric pressure anomalies are displayed in Supplementary Fig. 11. Sea level oscillations were significant with a signal to noise ratio of >2 at tide gauges as far north as Portland, ME (station 36).

Within Delaware Bay, tide gauges at Lewes, DE, Ship John Shoal, NJ, and Cape May, NJ all have positive first arrivals of the observed sea level oscillation. With an average wavelength on the order of 150 km, the pressure anomaly may be too wide to exert its force fully on Delaware Bay, which has a maximum width of 60 km. The maximum water depth in the bay is 30 m[20], corresponding to a maximum shallow water wave speed of ~17.1 m s^{-1}. This speed is lower than the forward speed of the atmospheric pressure anomaly during the first MCS (~22 m s^{-1}) over the bay, implying a supercritical flow regime, in which a positive sea level anomaly corresponds to a positive atmospheric pressure anomaly (Method), as observed at the tide gauges in the bay (Fig. 5, Supplementary Fig. 10, Supplementary Fig. 12). Further investigation, perhaps using a numerical model, is required to determine the relative importance of atmospheric pressure and wind forcing within Delaware Bay.

The second MCS propagated eastward over the continental U.S. and subsequently propagated across the Atlantic Ocean. Lewisetta, VA (station 9), well within Chesapeake Bay, was the first NOAA tide gauge to detect the second MCS atmospheric pressure anomaly and wind gusts (Supplementary Fig. 13). The MCS crossed over this gauge at 1942 UTC, with a sea level oscillation occurring shortly after at 2000 UTC. The longest delay time for the second meteotsunami occurred at the tide gauge at Wachapreague, VA (station 10), outside Chesapeake Bay, with an arrival of the atmospheric pressure anomaly and strong wind gusts at 2042 UTC, followed by a sea level oscillation arriving at 2242 UTC. However, most delay times between the second MCS atmospheric pressure anomaly (as well as wind gusts) and recorded sea level oscillations were less than an hour for stations south of Atlantic City, NJ (Fig. 5). This short delay time supports the working hypothesis that within Chesapeake Bay, sea level oscillations are created under direct forcing (in shallow water near the tide gauge stations), not reflections off the shelf break. Since the width of Chesapeake Bay (~25 km) is much less than the average wavelength of the atmospheric pressure anomaly (~150 km), the sea level oscillations are most likely the result of wind stress, not atmospheric pressure forcing.

Outside the two bays towards the open ocean, the increasing water depth on the continental shelf leads to a higher shallow water wave speed that approaches the propagation speed of the MCS near the continental shelf break, resulting in growing amplitude of the water wave. Mercer et al.[2] illustrate with a numerical model that a meteotsunami moving over a shelf break into deeper water has both transmitted and reflected wave energy. Once the meteotsunami is reflected, it travels as a free wave. Indeed, in the present study, sea level oscillation arrivals for stations 19–30 (north of and including Atlantic City) are consistent with the predicted travel times[21] of

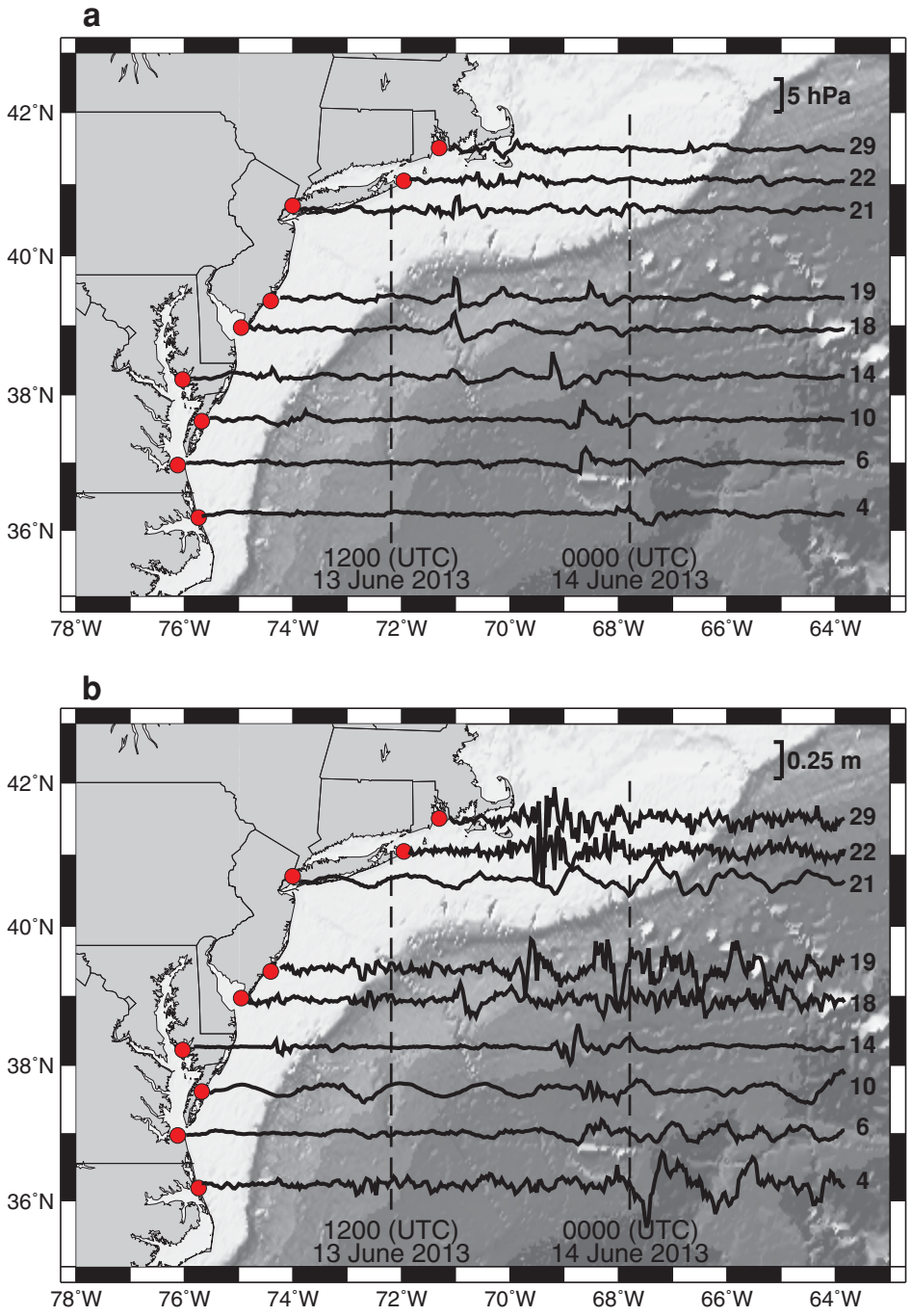

Figure 5 | (a) Atmospheric surface pressure anomalies and (b) corresponding sea level oscillations for all 38 NOAA tide gauge stations. Tide gauge station locations (red circles) and numbers are listed in Table 1 and displayed here. Maps were created with software Generic Mapping Tools (GMT v4.5.12; http://gmt.soest.hawaii.edu).

waves reflected from the shelf break (Supplementary Fig. 14; Method).

The first arrival of a sea level anomaly at NOAA Deep-ocean Assessment and Reporting of Tsunamis (DART) buoy 44402, east of the shelf break, is the first meteotsunami transmitted across the shelf break, moving at a shallow water wave speed that causes it to arrive before the atmospheric pressure anomaly (Fig. 6). DART instruments are ocean pressure sensors located on the seafloor that report ocean pressure as water column height[22]. The instruments record every 15 minutes unless the sea level oscillation exceeds one of two critical thresholds, at which time sampling increases to every minute or 15 seconds. Removing the mean water depth and high-pass filtering low-frequency oscillations over 5 hours reveals two sea level anomalies that passed over the station, the first at 1654 UTC and the second at 2006 UTC on June 13, 2013. Unlike the NOAA tide gauges, the first wave event occurred before high radar reflectivity of the first MCS passed over the station, suggesting that the leading edge of the meteotsunami propagated faster than the atmospheric forcing (Fig. 6b). The second arrival at DART buoy 44402 occurred three hours later, with a reversed polarity. The first arrival is attributed to the transmitted wave from the continental shelf break, and the second arrival is attributed to a wave that was first reflected from the continental shelf break, then reflected again at the shoreline, and finally transmitted across the continental shelf break to DART buoy 44402. To estimate the time between the transmitted arrival at the buoy and the reflected arrival, a travel time model[21] is used with a

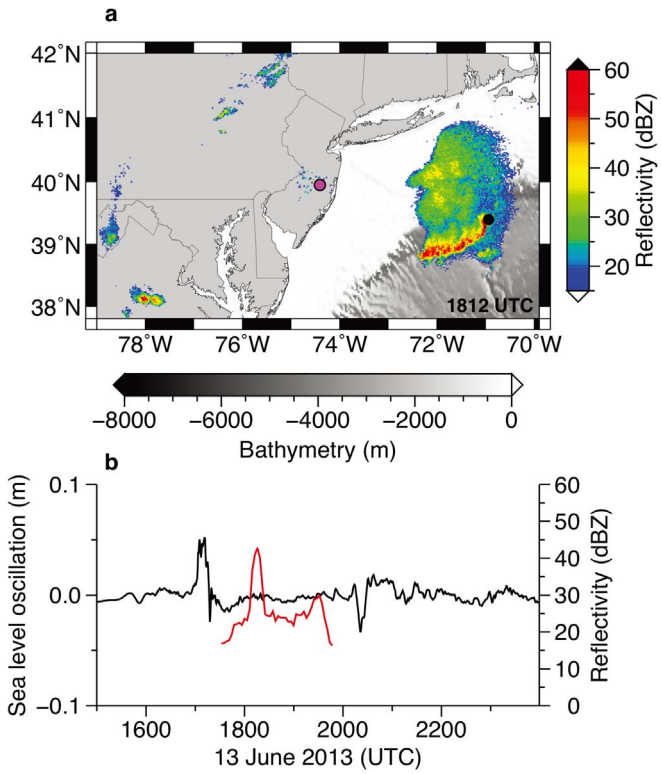

Figure 6 | Response to atmospheric forcing observed at DART buoy 44402. (a) NOAA WSR-88D KDIX radar reflectivity at 1812 UTC on June 13, 2013 near DART buoy 44402 (black circle) and the location of KDIX (magenta); (b) sea level oscillation (black) and radar reflectivity (red) time series on June 13, 2013, where the sea surface height is interpolated to every 1 minute, demeaned, and five-hour high-pass filtered. Map was created with software Generic Mapping Tools (GMT v4.5.12; http://gmt.soest.hawaii.edu).

shallow water velocity structure obtained using National Geophysical Data Center (NGDC) bathymetry[23] (Method). Results indicate that a majority of the energy reflected off the coastline would arrive back at the buoy ~3 hours after the transmitted meteotsunami arrives at the buoy (Supplementary Fig. 15), consistent with the observations of both the June 13, 2013 (Fig. 6b) and April 10, 2013 (Supplementary Fig. 16) meteotsunamis observed at DART buoy 44402.

Unlike the first MCS, the second MCS generated no significant meteotsunami reflection off the continental shelf break. Specifically, there were no significant sea level oscillations at stations north of Atlantic City, NJ, and no significant sea level oscillation was detected by DART Buoy 44402 or 41424 in response to the second MCS. The second MCS decelerated to a propagation speed of ~20 m s^{-1} and then to 15 m s^{-1} (Fig. 4) as it propagated towards the shelf break, which limited the region of Proudman resonance along the shelf and reduced the amplitude of the second meteotsunami in areas decoupled from the atmospheric pressure forcing.

Discussion

The observed correlation between radar reflectivity and atmospheric pressure anomalies recorded by TA and tide gauge stations (Figs. 2 and 3) indicates that the largest positive pressure anomalies occur where reflectivity is >40 dBZ. These areas also experience mesolows before and after passage of the convective line of the MCS. The integrated area over the continental shelf that has reflectivity > 40 dBZ is 40,000 km^2 during five hours for the first MCS and 90,000 km^2 during 20 hours for the second MCS, as indicated by NOAA WSR-88D stations KDIX, KAKQ, and KMHX. Although the second MCS covered ~2 times the area of the first MCS, the duration of the second MCS was four times as long due to its slower propagation speed and larger spatial extent. This speed disparity causes the atmospheric pressure forcing by the second MCS to be less efficient than the first MCS for generating a large amplitude water wave along the continental shelf.

The absence of a detected shelf break meteotsunami reflection from the second MCS at coastal tide gauge stations suggests that there may be a minimum threshold for the size of the MCS forced area under Proudman resonance that is required to observe a meteotsunami reflected off the shelf break. To find where the meteotsunamis were most efficiently generated, the area where resonance is occurring is defined to be the area where the MCS propagation speed and the shallow water wave speed are similar ($0.707 < U/C < 1.225$), as indicated by the yellow-colored regions in Fig. 7. These values correspond to where the absolute amplitude of the water wave is ~2 times the magnitude of the response to a stationary pressure anomaly (Method). The second MCS covers a larger area over the continental shelf than the first MCS does. However, 35% of the area covered by the first MCS and a much smaller percentage of the area covered by the second MCS (10%) are resonant. The lower percentage for the second MCS indicates that the speed of the second MCS was not as optimal for generating a meteotsunami through Proudman resonance. For the first MCS, the resonant region was a continuous strip at latitude 39–40°N near the continental shelf break. For the second MCS, the resonant region was distributed over a much larger latitude range (33–40°N) in relatively small patches. The smaller, noncontiguous patches may indicate a reduced pressure anomaly relative to the first MCS. In addition, those patches occurred at different times, further distributing the sea level oscillations over time and limiting their amplitudes.

By examining the entire MCSs as they pass over the Atlantic Ocean, the areas that are approximately resonant and the amount of time spent in resonance are estimated (Fig. 7; Supplementary Fig. 17). These areas provide constraints on the possible locations of the reflection of tsunami waves along the continental shelf break. The second MCS crossed over both a broad continental shelf break at ~33–34°N and a narrow shelf to the north, while the first MCS crossed over a narrow shelf break at ~39–40°N (Fig. 7). The broad shelf break traversed by the second MCS allowed more wave energy to be transmitted across the shelf break than reflected back towards the coast[24], contributing to a relatively weak reflected meteotsunami and negligible sea level oscillations being recorded at the South Carolina tide gauges in response to the forcing from the second MCS. Within local bays and harbors north of 34°N, detecting a signal associated with reflection of the second meteotsunami is difficult because the signal is embedded within the noise associated with the oscillations or seiches generated by the first meteotsunami.

Land-based radar reflectivity extends to ~230 km, limiting the extent that MCSs can be observed off the coast. However, for near-term meteotsunami prediction, radar-based observations (supplemented whenever possible by coincident *in situ* atmospheric surface pressure measurements) only need to be made as an MCS passes over resonant areas, which are within this 230 km limit for MCS propagation speeds < 40 m s^{-1}. Most of the resonant areas for typical MCS propagation speeds of 20–40 m s^{-1} are within 200 km of the coast. Once the meteotsunami is in a subcritical regime, it outruns the atmospheric forcing, traveling at the local shallow water speed. At this point, predictions must rely on models to estimate reflections off the continental shelf and back towards the coastline. Radar is most helpful for tracking and estimating the MCS velocity as it propagates offshore.

One potential limitation of this study is the assumption that the wind stress forcing is negligible compared to the atmospheric pressure forcing[25]. Although wind stress is known to affect the magnitude

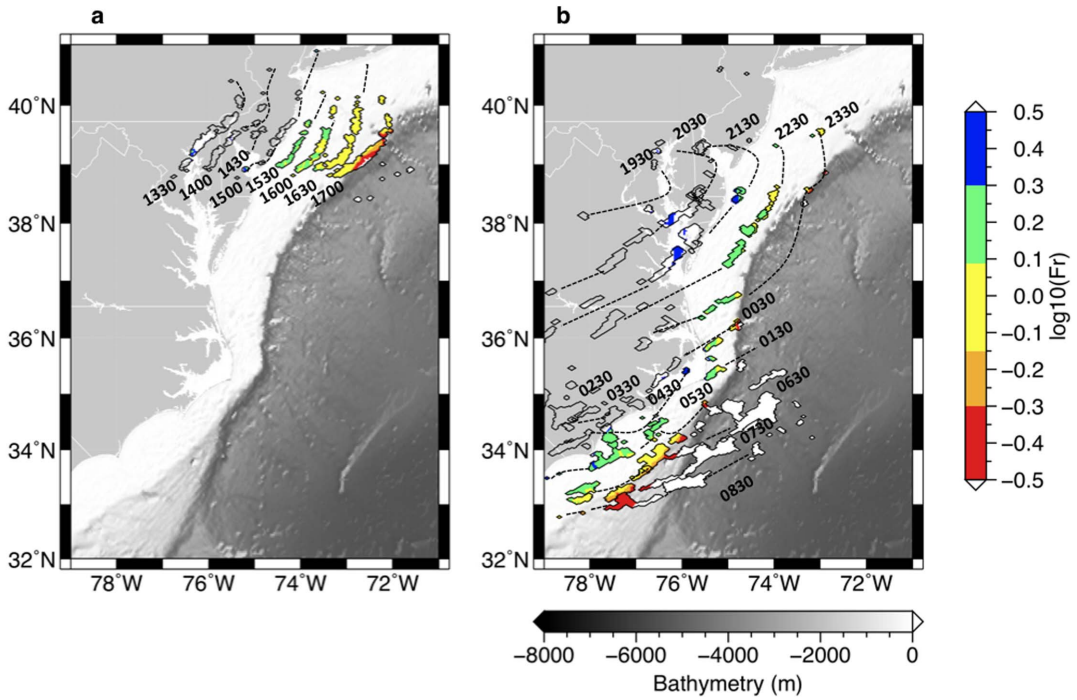

Figure 7 | Location of Proudman resonance and high radar reflectivity for the meteotsunami generated by the first and second MCS. Contours of reflectivity above 40 dBZ, determined from NOAA WSR-88D stations KDIX, KAKQ and KMHX, are colored according to the corresponding log10(U/C). Time (UTC) on June 13-14, 2013 is contoured for the (a) first MCS and (b) the second MCS. Maps were created with software Generic Mapping Tools (GMT v4.5.12; http://gmt.soest.hawaii.edu).

of the shallow water wave, this effect is likely to be small relative to the atmospheric pressure forcing outside of shallow bays because the effect of wind stress is inversely proportional to water depth. Within Chesapeake Bay, due to the small crossing distance, wind forcing is likely the dominant mechanism for generating the observed sea level oscillations. Oscillation generation mechanisms within Delaware Bay are harder to determine. For example, stations at Lewes, DE and Cape May, NJ, located on opposite sides of Delaware Bay (Supplementary Fig. 12), support a primarily pressure-driven sea level oscillation, as indicated by the positive and equal amplitude of the initial sea level oscillations; if the wind stress contribution was significant, then the westerly wind stress associated with the eastward-propagating MCS should increase the sea level oscillation magnitude at Cape May, NJ relative to Lewes, DE. This increase, however, is not observed.

Since meteotsunamis generated by MCSs along the U.S. East Coast are damaging to property, hazardous to boats in shallow waters, and dangerous to public safety, predicting these events is of financial and social value. The U.S. East Coast continental shelf and bays are environments where two wave trains created by the same meteotsunami-producing event can be present. The first wave train is forced directly beneath an atmospheric pressure anomaly and strong wind gusts, as seen at the stations in Delaware and Chesapeake Bay on June 13, 2013, and the second wave train results from the reflection of the wave off the continental shelf break, seen at the stations along the Atlantic coast and in Narragansett Bay on that day. This double wave train phenomenon has not been observed in other areas of the world where meteotsunamis have been documented[1–5].

For near-term meteotsunami prediction along the U.S. East Coast, three stages in the forecast process are suggested: (1) using land-based pressure measurements to monitor the magnitude of the atmospheric surface pressure anomalies as a radar-indicated MCS propagates towards the coast from the interior of the U.S., (2) monitoring radar reflectivity as the MCS propagates off the coast to the potential geographical area where Proudman resonance may occur, and (3) modeling of the meteotsunami development and possible reflection off the shelf break back towards the coastline.

Developing and then operationally implementing accurate numerical models of meteotsunami waves under atmospheric pressure (and perhaps wind) forcing is the next step towards understanding and predicting when and where MCS-generated meteotsunamis may occur. Ports, harbors, and bays may all have varying risk, and characterizing areas that may have extreme resonant mechanisms is also required. Places like Atlantic City, NJ, documented both in the present study and in others[7], appear to have an especially large ocean response to MCS forcing. Along with numerical modeling, monitoring high-frequency atmospheric pressure anomalies in the interior of the continental U.S. and along the coastline is essential for early warning of potentially hazardous meteotsunamis.

Method

Pressure and Radar Anomaly Location. Estimates of the center of the atmospheric pressure anomalies and radar reflectivity of the first MCS front were found using pressure data from the TA stations and NOAA/WSR-88D radar station KPBZ. Station KPBZ was used because of the dense coverage of TA stations surrounding it. Atmospheric pressure time series were demeaned, high pass filtered over 5 hours, and squared so positive and negative anomalies did not cancel. Pressure data were averaged a half an hour before and after a given time step and then linearly interpolated to a 10 km grid. Radar data were down-sampled to a 10 km by 10 km grid. Radar reflectivity >40 dBZ was used to isolate the MCS front. The centers of the pressure anomalies and radar reflectivity measurements were calculated at five-minute intervals using a gray-level-weighted average of values. Results are displayed in Supplementary Fig. 7.

MCS Propagation Speed. The propagation speed and back-azimuth of the two MCSs are based on NOAA WSR-88D radar reflectivity > 40 dBZ (primarily within the convective line) from station KDIX for the first MCS and KMHX for the second MCS. A 2-D cross-correlation of two successive reflectivity images is performed. To obtain estimation errors, estimations are performed over multiple time steps ranging from 5 minutes to 1 hour. The MCS propagation direction is estimated from the spatial shift of the peak cross-correlation, and the speed is calculated from the distance of the peak cross-correlation shift divided by the time interval between the reflectivity images.

Propagation speed and back-azimuth of the atmospheric pressure anomalies are found using the center of the pressure anomalies described above. Instead of a 2-D

cross correlation, the change in position of the center of the pressure anomaly over a known time is calculated to find velocity. To obtain error estimations, speeds and back-azimuths are calculated using multiple time steps ranging from 5 minutes to 2 hours. Results during the first MCS from the atmospheric pressure anomalies, as well as the radar reflectivity, are displayed in Supplementary Fig. 8.

Proudman Resonance. The sea level anomaly (N) due to an atmospheric pressure anomaly (P_o) moving at a constant speed (U), neglecting bottom friction and the Coriolis effect, is given by[24]:

$$N = \left(\frac{P_0}{g\rho}\right) \Big/ \left(Fr^2 - 1\right) \quad (1)$$

where Froude number $Fr = U/C$, g is gravitational acceleration, and ρ is the water density. From equation (1), a positive (negative) atmospheric pressure anomaly yields a positive (negative) sea level anomaly under the supercritical condition ($Fr > 1$), where the pressure anomaly is moving faster than the tsunami waves. In contrast, a positive (negative) atmospheric pressure anomaly yields a negative (positive) sea level anomaly under the subcritical condition ($Fr < 1$), where the pressure anomaly is moving slower than the tsunami waves. As Fr approaches 1 (the critical condition), Proudman resonance occurs, resulting in a large sea level anomaly. The steady-state sea level anomaly becomes infinite when $Fr = 1$ in the idealized situation described by equation (1).

Reflected Travel Times. To estimate arrival times at tide gauges 19–30 (Supplementary Fig. 14), the travel time from positions on the shelf break underneath the first MCS to the tide gauges is calculated using a travel time model[21] with a shallow water velocity structure converted from NGDC bathymetry[22] and added to the time of reflection at the shelf break. NOAA WSR-88D radar reflectivity from station KDIX was used to estimate a reflection time of 1700 UTC for the meteotsunami (generated by and initially collocated with the first MCS) from the continental shelf break, defined as a depth of 140 m. The first MCS covered a latitudinal range from 39°–40°N.

Tsunami Travel Times. The travel time of rays from various back-azimuths and reflection points to the DART 44402 buoy are calculated using a travel time model[21] with a shallow water velocity structure obtained using NGDC bathymetry[22]. The time delay (T_D) between the transmitted and coast-reflected tsunami arrivals at the buoy is given by:

$$T_D = T_R - T_T \quad (2)$$

where T_R is the travel time from the continental shelf break to the shore and back to the buoy, and T_T is the travel time from the continental shelf break to the buoy. Here, the continental shelf break and the shore are defined as 140 m depth and 0 m depth, respectively.

1. Goring, D. G. Meteotsunami resulting from the propagation of synoptic-scale weather system. *Phy. Chem. Earth.* **34**, 1009–1015 (2009).
2. Mercer, D., Sheng, J., Greatbatch, R. J. & Bobanović, J. Barotropic waves generated by storms moving rapidly over shallow water. *J. Geophys. Res.* **107**, 1–17 (2002).
3. Monseratt, S., Vilibić, I. & Rabinovich, A. B. Meteotsunamis: atmospherically induced destructive ocean waves in the tsunami frequency band. *Nat. Hazards Earth Syst. Sci.* **6**, 1035–1051 (2006).
4. Thomson, R. E. *et al.* Meteorological tsunamis on the coasts of British Columbia and Washington. *Phy. Chem. Earth.* **34**, 971–988 (2009).
5. Haslett, S. K., Mellor, H. E. & Bryant, E. A. Meteo-tsunami hazard associated with summer thunderstorms in the United Kingdom. *Phy. Chem. Earth.* **34**, 1016–1022 (2009).
6. Proudman, J. The effects on the sea of changes in atmospheric pressure. *Geophys. J. Int.* **2**, 197–209 (1929).
7. Pasquet, S., Vilibić, I. & Šepić, J. A survey of strong high-frequency sea level oscillations along the US East Coast between 2006 and 2011. *Nat. Hazards Earth Syst. Sci.* **13**, 473–482 (2013).
8. Pasquet, S. & Vilibić, I. Shelf edge reflection of atmospherically generated long ocean waves along the central U.S. East Coast. *Cont. Shel Res.* **66**, 1–8 (2013).
9. Churchill, D. D., Houston, S. H. & Bond, N. A. The Daytona Beach wave of 3-4 July 1992: A shallow water gravity wave forced by a propagating squall line. *B. Am. Meteorol. Soc.* **76**, 21–32 (1995).
10. Bentley, M. L. & Sparks, J. A. A 15 yr climatology of derecho-producing mesoscale convective systems over the central and eastern United States. *Clim. Res.* **24**, 129–139 (2003).
11. Ashley, W. S. & Mote, T. L. Derecho hazards in the United States. *Bull. Amer. Meteor. Soc.* **86**, 1577–1592 (2005).
12. SPC severe weather event review for Thursday June 13, 2013, http://www.spc.noaa.gov/exper/archive/event.php?date=20130613 (2013) Date of access: 06/21/2013.
13. USArray Data at the DMC. http://www.iris.edu/earthscope/usarray (2013) Date of access: 07/22/2013.
14. CO-OPS specifications and deliverables for installation, operation, and removal of water level stations. http://beta.tidesandcurrents.noaa.gov/publications/CO-OPS_Specifications_and_Deliverables_for_installation_operation_and_removal_of_water_level_stations_updated_November2008.pdf (2008) Date of access: 10/15/2013.
15. Adams-Selin, R. D. & Johnson, R. H. Mesoscale surface pressure and temperature features associated with bow echoes. *Mon. Wea. Rev.* **138**, 212–227 (2010).
16. Houze Jr, R. A. Mesoscale convective systems. *Rev. Geophys.* **42**, 1–43 (2004).
17. Houze Jr, R. A., Rutledge, S. A., Biggerstaff, M. I. & Smull, B. F. Interpretation of Doppler weather radar displays of midlatitude mesoscale convective systems. *Am Meteor. Soc.* **70**, 608–619 (1989).
18. Vilibić, I. & Šepić, J. Destructive meteotsunamis along the eastern Adriatic coast: Overview. *Phys. Chem. Earth* **34**, 904–917 (2009).
19. Parker, B. B. Tidal analysis and predictions. http://beta.tidesandcurrents.noaa.gov/publications/Tidal_Analysis_and_Predictions.pdf (2008) Date of access: 10/15/2013.
20. Multibeam Bathymetry. http://www.ngdc.noaa.gov/mgg/bathymetry/ (2013) Date of access: 07/19/2013.
21. Margrave, G. F. Numerical methods of exploration seismology with algorithms in MATLAB. http://www.crewes.org/ResearchLinks/FreeSoftware/NumMeth.pdf (2003) Date of access: 10/27/2013.
22. Deep-ocean assessment and reporting of tsunamis (DART®) Description. http://www.ndbc.noaa.gov/dart/dart.shtml (2013) Date of access: 09/15/2013.
23. Amante, C. & Eakins, B. W. ETOPO1 1 Arc-minute global relief model: procedures, data sources and analysis. NOAA Technical Memorandum NESDIS NGDC-24. http://www.ngdc.noaa.gov/mgg/global/relief/ETOPO1/docs/ETOPO1.pdf (2009) Date of access: 07/19/2013.
24. Kowalik, Z. Introduction to Numerical Modeling of Tsunami Waves. https://www.sfos.uaf.edu/directory/faculty/kowalik/Tsunami_Book/book_sum.pdf (2012) Date of access: 01/10/2014.
25. Dean, R. G. & Dalrymple, R. A. *Water wave mechanics for engineers and scientists* (World Scientific Publishing Co., New Jersey 1991).

Acknowledgments

We thank NOAA for providing the buoy data and NSF for supporting the USArray Transportable Array. We also thank the various institutions who participated in the July 18, 2013 teleconference to discuss ideas and preliminary analysis of the June 13, 2013 tsunami event along the U.S. East Coast, which the URI team had previously identified as being caused by MCS pressure forcing. This project is partially supported by the University of Rhode Island Council for Research Funds. Materials from the July 18, 2013 teleconference are available online at: http://nctr.pmel.noaa.gov/eastcoast20130613/.

Author contributions

C.A.W. gathered and analyzed data. R.M.Y. analyzed radar data and identified MCSs as the most likely source for the tsunami-like oscillations. Y.S. analyzed seismic data and ruled out offshore earthquakes as a possible source for the tsunami-like sea-level oscillations. J.M. investigated the relevance of Proudman resonance as a key contributor to the magnitude of the sea-level oscillations. C.A.W., R.M.Y., Y.S., J.M. C.R.K. and R.A.P. discussed the results and implications and commented on the manuscript and Supplementary Information at all stages.

Additional information

Supplementary information accompanies this paper at http://www.nature.com/scientificreports

Competing financial interests: The authors declare no competing financial interests.

How to cite this article: Wertman, C.A. *et al.* Mesoscale convective system surface pressure anomalies responsible for meteotsunamis along the U.S. East Coast on June 13th, 2013. *Sci. Rep.* **4**, 7143; DOI:10.1038/srep07143 (2014).